Analysis of Connected Shallow Arches under a Load from a Moving Rigid Wedge

Priyabrata Maharana[1] and G. K. Ananthasuresh[1]

[1] Mechanical Engineering, Indian Institute of Science, Bengaluru
{priyabratam, suresh}@iisc.ac.in

Abstract. In this paper, we analyze a pair of shallow arches that are interconnected with each other through their ends by a revolute joint. The other ends of the arches may be pinned or fixed. The two arches have opposite curvature. When one of the arches is subjected to a transverse load, it deforms and eventually flips to its inverted shape. Simultaneously, the deformation of the first arch triggers the switching of the second arch due to a moment transfer between the two arches through the revolute joint, and the second arch flips to its inverted shape too. These arches can be switched back to their as-fabricated shape by applying a transverse load to the second arch. In this way, these connected arches move up and down to take the load at any instant when the switching loads come from a long moving rigid wedge. The motivation to study such connected flipping arches arose from the intent to develop dynamically self-offloading footwear for diabetics suffering from peripheral neuropathy. The purpose of this is to limit the plantar pressure to stay below a prescribed value to prevent ulceration. When a certain region of the sole is offloaded, the array of connected arches help certain other region to take up the differential load to support the body weight. In this paper, we present a theoretical formulation for two connected arches, solve them semi-analytically, and compare with the results of the geometrically nonlinear finite element analysis.

Keywords: Snap through • Post-buckling • Self-offloading footwear.

1 Motivation for studying connected arches

Peripheral neuropathy, i.e., nerve damage that causes loss of sensation, pain, and numbness, is one of the major complications of diabetes. The lack of sensation in the sole of the feet leads to ulceration and recurring wounds which, if left untreated, necessitate amputation of the feet [1]. This can be easily prevented by using offloading footwear to protect vulnerable regions of the sole. The current clinical practice is to measure the plantar pressure of a patient using pedoscan to identify regions of high pressure and to prescribe customized in-soles. As shown in Figs. 1a-b, either a pocket is carved out in a foam-like material used as the in-sole, or it is contoured to transfer the load to other regions. This is called *static offloading* of the plantar pressure as the high-pressure regions of the sole of the foot are offloaded fully or partially. When a certain region of the sole is thus offloaded, certain other region becomes vulnerable as they bear a larger portion of the body weight. Therefore, ulceration begins elsewhere warranting frequent modification of the in-sole of the footwear. One way to prevent this is to design dynamically offloading footwear that automatically re-distributes the body load evenly on the

sole during the entire gait cycle. We had proposed such *self-offloading footwear* by using snapping arches [2] whose concept is depicted in Fig. 2.

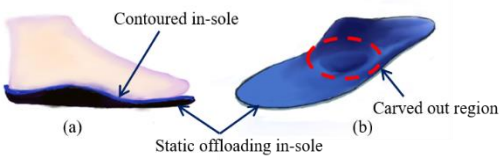

Fig. 1. Static offloading in-sole used in current practice: (a) a contoured in-sole for even distribution of pressure; and (b) in-sole with a carved-out region if there is an ulcer.

Four phases of the gait cycle, namely, *heel strike*, *midstance*, *flat foot*, and *heal off*, are shown in Fig. 2a. The manner of offloading is also shown for three types: (i) static offloading, (ii) self-offloading with unconnected arches, and (iii) self-offloading with inter-connected arches. In static offloading, the plantar pressure distribution is pre-set and remains mostly unchanged. As stated above, this has the drawback of creating high-pressure regions elsewhere. In self-offloading using connected arches [3], the arches (shown in red color in Fig, 2a) snap down along with the deformable in-sole (shown in blue color) such that no region would take up more than the prescribed level of plantar pressure. While this helps to some extent, further improvement is possible if the arches transfer the load to other arches to evenly distribute the body weight. This is possible in interconnected arches as depicted in Fig. 2b, wherein the left and right arches flip-flop up (i.e., they move and down) when the load from the foot (considered as a moving rigid wedge) changes in the walking cycle.

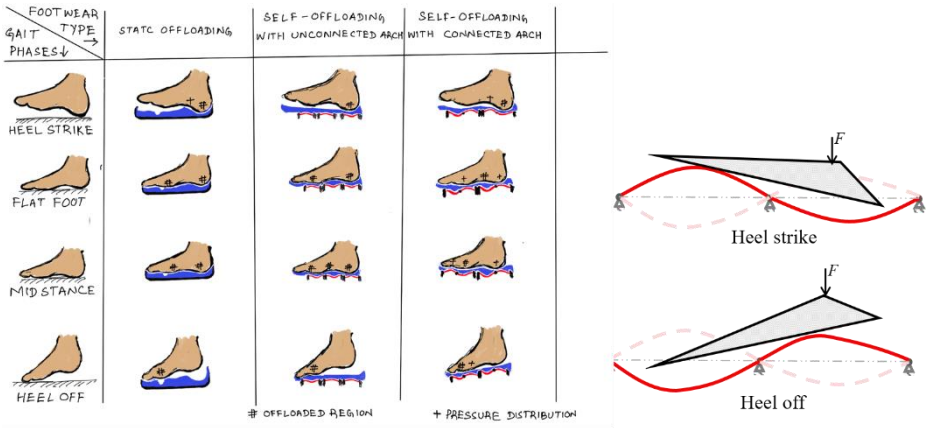

Fig. 2. (a) Comparison of static offloading footwear, self-offloading footwear with unconnected arches, and self-offloading footwear with inter-connected arches during four phases of the gait cycle, namely, *heal strike*, *flat foot*, *midstance*, and *heal off*. The symbol **#** shows the offloaded regions, and **+** shows the pressure-redistributed regions during offloading. (b) Flip-flop of the connected arches in heel strike and heel off phase. The dashed line denotes the configurations before switching at the beginning of the particular gait phase.

In our earlier work, we have conceptualized and implemented self-offloading with unconnected arches [2-3]. As shown in Fig. 3a, by placing the in-sole over an array of arches (see Fig. 3b), offloading can be achieved whenever the pressure at a point exceeds the allowed limit (210 kPa in adults). In this arrangement, the arches undergo snap-through by losing contact with the sole of the foot when the load on them is beyond the preset threshold, as shown in Fig. 3d. The arches are designed in such a way that they snap back up during a different phase of the gait cycle. This is illustrated in Fig. 3a wherein the in-sole is supported by four capping plates under which there are arrays of snapping arches and top of which there are two layers of soft-soles to absorb the shock from the in-sole (see Fig. 3c). This prototype was tested at Karnataka Institute of Endocrinology and Research (KIER), Bengaluru. It was found that the self-offloading footwear reduces the peak pressure by about 34% while keeping the plantar pressure during the complete gait cycle below 210 kPa [3]. It was also observed that further reduction in plantar pressure is possible if the capping plates are interconnected so that they can redistribute the load dynamically among them rather than only offloading individually. This is the motivation for the current study of connected arches.

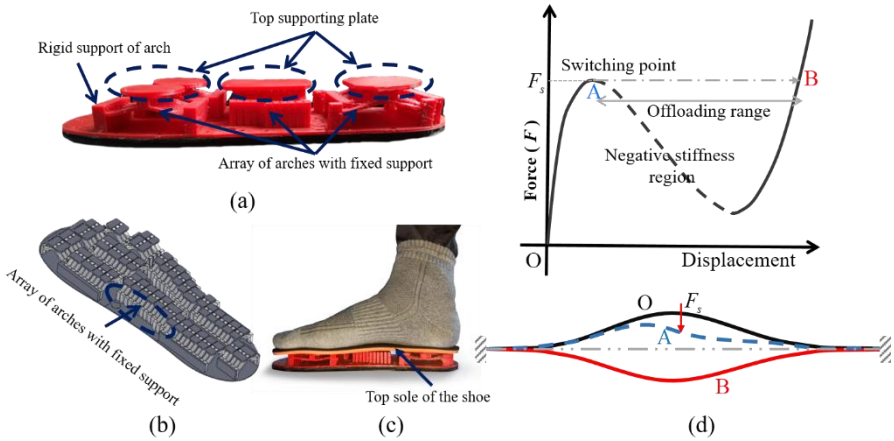

Fig. 3. (a) A self-offloading in-sole using an array of snap-through arches beneath the capping plates, (b) CAD model of the in-sole showing array of fixed-fixed arches, (c) 3D-printed prototype with two layers of top sole (black and orange) to absorb the shock from the in-sole, and (d) force-displacement curve of snap-through arch showing the as-fabricated shape (O), shape at the switching point (A), and the inverted shape (B) after offloading.

1.1 Scope of the paper

As a first study, in this paper, we consider two arches connected with a revolute joint and analyze their snapping behavior. We model the foot as a rigid wedge that comes into contact with the arches at different points during the gait cycle. As a further simplification, we consider the force from the foot only at the midpoints of the two arches.

In this paper, we present a semi-analytical method to investigate the characteristics of planar-connected arches when the two arches have either hinged-hinged or fixed-hinged boundary conditions. This is beneficial in two ways: (i) finite element analysis

involves considerable computation because of the inherent geometric nonlinearity, whereas the semi-analytical method will be much faster, which leads to a quicker way to know if the arches undergo flip-flop, and (ii) the analytical method paves the way for closed-form relationships in synthesis of the arch shapes for desired behavior as was done in [4, 5].

We introduce a compatibility condition for the deformed arch profiles of the connected arches such that they maintain the continuity slope at the common revolute joint. We obtain the equilibrium equations of such arches using the potential energy and the derived compatibility condition. We numerically solve these equilibrium equations to get the force-displacement characteristics for the loading and unloading cycle and understand the switching and bistability criteria for different kinds of arch profiles. This analysis helps us in understanding the nature of the connected arches as well as designing them by choosing suitable arch geometry for various applications.

Pre-buckling a straight beam into an arch [6] and arriving at a suitable stress-free arch shape [7-10] are the two ways to get an arch structure. Based on the geometry and boundary conditions, an arch can show either snap-through or bistability phenomena. This nature of the arch is characterized by the physical quantities, like the *switching force*, the *switchback force*, and the *travel* of the arch. These quantities are identified from the nonlinear force-displacement characteristics of the arch. Knowing these quantities helps us in designing the arches for various applications by suitably choosing the arch dimensions. The analysis for fixed-fixed and pinned-pinned arches with general boundary conditions were presented by Qiu et al. [7], and design methods by Palathingal and Ananthasuresh [10], to identify these physical quantities for an arch of arbitrary as-fabricated stress-free shape. The as-fabricated shape of the arch highly influences the bistable nature of the arch. Therefore, Palathingal and Ananthasuresh [4, 5] presented an analytical way of finding bilateral relationships between the two stable configurations of the arch. They also mentioned sufficiency criteria based on which one can decide the stability of the arches. Though the literature is rich with the analysis of single arches, there is no literature available for an arrangement where two arches are connected through a revolute joint between them, as shown in Fig. 4. But some of the earlier works reported on the analysis of continuous linear beams [9] and periodically connected linear beams [11]. When two arches are connected, one arch acts as a nonlinear spring for the other, and vice versa, due to the coupling of the slope at the common joint.

In Section 2, we derive the potential energy, compatibility condition, and the equilibrium equation for the analysis. In this section, we also explain the force-displacement characteristics with a suitable example of pinned-pinned arches, and discuss the switching and stability criteria of connected arches. The results of the analytical model are compared with finite element analysis solution done using ABAQUS finite element analysis software (www.simulia.com) and presented in Section 3. Summary and concluding remarks of the work are included in the last section.

2 Analysis of connected arches

We consider arches with either pinned-pinned or fixed-pinned boundary conditions for the analysis. Let us take two arches of span, L, depth, d, breadth, b that are connected

with each other through a common revolute joint in between them as shown in Fig. 4. The mid-span height of the left arch is taken to be h_{mid} where a point load, f is applied. The main question we ask is this: Under what conditions, would the second arch flip up when the first arch experiences a load to switch it down?

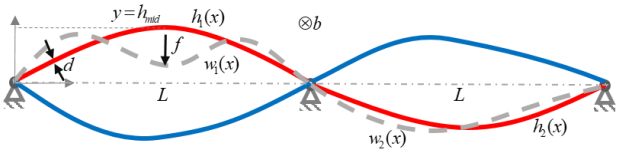

Fig. 4. Connected pinned-pinned arches with all the dimensions showing the as-fabricated shape (red-solid), intermediate deformed shape (grey-dashed), and inverted stable shape (blue-solid)

We begin the analysis by representing the as-fabricated stress-free state, $h_i(x)$, and the deformed shape, $w_i(x)$ of the arches as a linear combination of the buckling mode weights of the corresponding straight beam as follows [8, 9]:

$$h_1(x)=h_{mid}\sum_1^N a_i\varphi_i\,;h_2(x)=h_{mid}\sum_1^N b_i\varphi_i\,;w_1(x)=h_{mid}\sum_1^N A_i\varphi_i\,;w_2(x)=h_{mid}\sum_1^N B_i\varphi_i \tag{1}$$

where φ_i is the mode shape that satisfies the boundary conditions of the arch. For a pinned-pinned arch, the mode shapes are [9]:

$$\varphi_i=\sin\left(i\pi\tfrac{x}{L}\right) \tag{2}$$

and for a fixed-hinged arch mode shapes are [9]:

$$\varphi_i=\cos\left(M_i\tfrac{x}{L}\right)-\frac{\sin\left(M_i\frac{x}{L}\right)}{M_i}+\frac{x}{L}-1 \tag{3}$$

where $M_i=1.43\pi,2.45\pi,3.47\pi,\cdots$ for $i=1,2,3,\cdots$. For a given as-fabricated mode weight, a_is and b_is, we determine the deformed-profile mode weights, A_is and B_is by minimizing the total potential energy of both the arches.

Total potential energy. For arches of Young's modulus, E, and second moment of area, I, the total bending strain energy is given by

$$SE_b=\frac{1}{2}EI\sum_{i=1,2}\int_0^L\left(\frac{d^2h_i}{dx^2}-\frac{d^2w_i}{dx^2}\right)^2dx \tag{4}$$

As we take the arches to be shallow, i.e., $\left(\frac{dh_i}{dx}\right)^2\ll 1$ and $\left(\frac{dw_i}{dx}\right)^2\ll 1$, the nonlinear terms in the bending energy are neglected. When the arches deform in the transverse direction, they develop axial compression, and the net strain energy due to the compression is expressed as

$$SE_c=\frac{1}{4}\frac{Ebd}{L}\sum_{i=1,2}\left\{\int_0^{L_1}\left[\left(\frac{dh_i}{dx}\right)^2-\left(\frac{dw_i}{dx}\right)^2\right]dx\right\}^2 \tag{5}$$

A point load, f, is applied at the mid-span length of the left-side arch. The work potential due to the transverse displacement of the point of application of the load is given by

$$WP=-f\left[h_1\left(\tfrac{L}{2}\right)-w_1\left(\tfrac{L}{2}\right)\right] \tag{6}$$

The total potential energy of the connected arches includes the strain energy due to bending, compression, and the work potential. It is expressed as

$$PE = SE_b + SE_c + WP \tag{7}$$

To get the equilibrium equations, we minimize the potential energy w.r.t. the unknown mode weights, A_is and B_is for left and right arches, respectively.

2.1 The compatibility condition

Due to the interconnection of the arches through the common revolute joint, the deformation of the left arch causes the deformation of the right arch even though it does not experience any external loading and vice versa. As the revolute joint does not resist the rotation of the arch, the deformed shape of both the arches maintains slope continuity at this point. In other words, the rotation of the left arch and the right arch are the same w.r.t. their as-fabricated states at the common revolute joint. Therefore, we impose a rotational compatibility condition at the interconnected revolute joint as:

$$\Theta = \frac{\left(\frac{dw_1}{dx}\Big|_L\right) - \left(\frac{dw_2}{dx}\Big|_0\right)}{1 + \left(\frac{dw_1}{dx}\Big|_L\right)\left(\frac{dw_2}{dx}\Big|_0\right)} - \frac{\left(\frac{dh_1}{dx}\Big|_L\right) - \left(\frac{dh_2}{dx}\Big|_0\right)}{1 + \left(\frac{dh_1}{dx}\Big|_L\right)\left(\frac{dh_2}{dx}\Big|_0\right)} = 0 \tag{8}$$

where the term containing $h_i(x)$s represents the tangent of angle difference, θ_0, between the as-fabricated shape of two the arches at the revolute joint, as shown in Fig. 5. When the arches are identical and have opposite curvature, Eq. (8) reduces to

$$\Theta = \left(\frac{dw_1}{dx}\Big|_L\right) - \left(\frac{dw_2}{dx}\Big|_0\right) = 0 \tag{9}$$

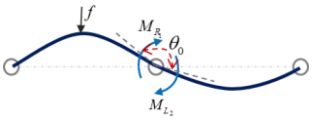

Fig. 5. A connected arch with the reaction moment and the initial angle difference of as-fabricated shape at the revolute joint.

The constraint condition at the common revolute joint eventually leads to concentrated moments, M_{R_1}, on the right end of left arch and M_{L_2}, on the left end of the right arch. Due to the revolute joint, both the moments cancel each other, and the net moment at the point becomes zero, i.e.,

$$M_{R_1} = -M_{L_2} \tag{10}$$

We get the equilibrium configuration of the arch by minimizing the potential energy such that the deformed profile of the arch satisfies the compatibility condition (Eq. (8)).

2.2 Equilibrium equations for connected pinned-pinned arches

In this section, we analyze the pinned-pinned connected arches, obtain the governing equilibrium equations, and study the force-displacement characteristics of the connected arches. We substitute Eq. (1) and (2) in Eq. (4) to (6) to get the potential energy expression, and minimize the potential energy (Eq. (7)) w.r.t. the unknowns A_is and B_is along with the compatibility condition (Eq. (8)) to get the governing equation of the connected arches as:

$$\frac{\partial(PE+\Lambda\Theta)}{\partial A_i}=\frac{M_i^4}{2}(A_i-a_i)-\frac{3}{2}Q^2C_1\left(A_iM_i^2\right)+F\left\{-(-1)^{\frac{i-1}{2}}\right\}\Big|_{i=1,3,5,\ldots}+\Lambda\left[\left\{(-1)^iM_i\right\}+\tan(\theta_0)\left\{\frac{h_{mid}}{L}\left[(-1)^iM_i\right]\left[\sum_1^N B_iM_i\right]\right\}\right]=0 \quad (11)$$

$$\frac{\partial(PE+\Lambda\Theta)}{\partial B_i}=\frac{M_i^4}{2}(B_i-b_i)-\frac{3}{2}Q^2C_2\left(B_iM_i^2\right)+\Lambda\left[-M_i+\tan(\theta_0)\left\{\frac{h_{mid}}{L}M_i\left[\sum_1^N A_iM_i(-1)^i\right]\right\}\right]=0 \quad (12)$$

$$\frac{h_{mid}}{L}\left\{\sum_1^N A_iM_i(-1)^i\right\}-\frac{h_{mid}}{L}\left\{\sum_1^N B_iM_i\right\}+\tan(\theta_0)\left\{1+\frac{h_{mid}^2}{L^2}\left\{\sum_1^N A_iM_i(-1)^i\right\}\left\{\sum_1^N B_iM_i\right\}\right\}=0 \quad (13)$$

where $M_i=i\pi$, $C_1=\sum a_i^2M_i^2-\sum A_i^2M_i^2$, $C_2=\sum b_i^2M_i^2-\sum B_i^2M_i^2$, $F=\frac{fL^3}{EIh_{mid}}$ is the nondimensional force on the arch and Λ is the multiplier corresponding to the continuity equation. Here, the multiplier (Λ) is equivalent to the internal moment at the common revolute joint due to the relative arch deformation. To understand the nature of the force-displacement, i.e., f-δ, characteristic of the connected arch, we numerically solve the preceding set of equations (Eq. (11) to (13)) and trace the curve for a range of displacement values for both loading and unloading cycles.

As an illustrative example, we take the as-fabricated shape of a connected arch consist only the first mode weights such that, $a_1=1$, and $b_1=-0.5$. We take $h_{mid}=10$ mm, $d=1$ mm, $b=4$ mm, $L=100$ mm, $E=50$ MPa, and substitute them in the equilibrium equations. Using Eq. (11) to (13), we solve f by varying δ from 0 mm to twice the height of the arch, i.e., 20 mm, to get the f-δ curve for the loading cycle. Similarly, to get the f-δ curve for the unloading cycle we vary δ in a reverse way. The force-displacement and mode weights-displacement characteristics of these connected arches are shown in Fig. 6.

In Fig. 6a, O represents the mid-point displacement at as-fabricated stress-free state and E represents that of the second force-free state. The arch follows the path OABCDEF (blue-solid curve) for the loading cycle and FECGAO (magenta-solid curve) for the unloading cycle. The loading and unloading pathways are different due to the asymmetric nature of the strain energy of the system. The initial phase, O-A, and the post-buckling phase, E-F are identical for both the loading and unloading cycle, whereas for a displacement between A and E, there are two different arch configurations and force values for the loading and unloading phases, leading to two different pathways.

When we increase the displacement gradually at point O, the magnitude of the first mode weights starts decreasing, and that of the second and third mode starts increasing for both the arches (see Fig. 6c-d). Although these arches and the loading condition are symmetric in nature, the arches deform asymmetrically due to the coupling at the common revolute joint. They act as a nonlinear rotational spring to each other, which leads to asymmetry in the system. As the load increases on the left arch, the slope at either end starts increasing. But due to the stiffness of the rotational spring of the right arch, the motion at the right end of the left arch gets restricted, and the slope at that point starts decreasing. This causes the second mode weight to increase on the positive side. With further increase in the displacement, the force value increases till the switching force value and decreases smoothly (curve O-A-B) till point B. At this point, the force and the stiffness suddenly jump to a lower value. This sudden jump occurs as the rotation of the right arch at the common revolute joint attains the switching rotation value

due to a point moment alone (see Fig. 6b), and the right arch switches to its inverted shape (see Fig. 6d-e). As shown in Fig. 6c, the second mode weight of the left arch attains a maximum at this point and starts decreasing gradually till the point D when the displacement is increased further. At this point D, the second mode weight for the left arch suddenly jumps (see Fig. 6e) and becomes negative (see Fig. 6c). This occurs due to the spring stiffening effect of the right arch. This stiffening also leads to a sudden increase in the force value, as shown in Fig. 6a. Further increment in the displacement also increases the force value on the arch. The same argument can also be made for the unloading path FECGAO when we vary the displacement in a reverse direction starting from the point F. We decide the nature of the connected arches based on their switching nature and stability at the inverted shape.

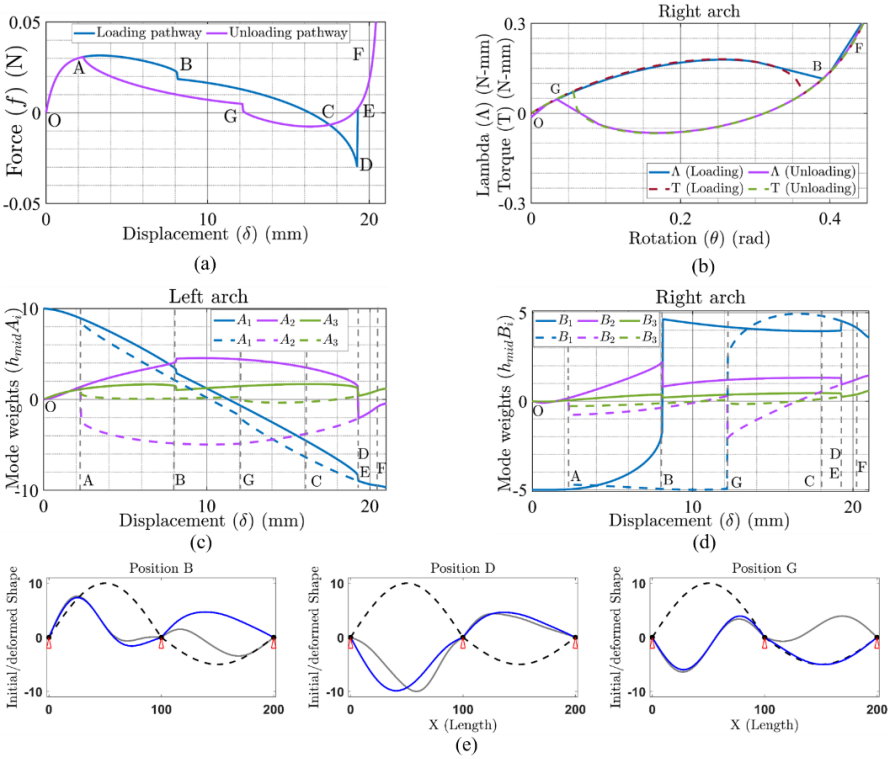

Fig. 6. (a) Force-displacement (f - δ) characteristics of the connected arch showing the loading path and the unloading path, (b) comparison loading and unloading pathways of torque (T)-rotation (θ) characteristics (solid curve) with the multiplier (Λ)-rotation (θ) characteristics (dashed curve) for the right arch. Note that a concentrated torque (T) is applied at the left end of the right arch, (c) mode weights variations of the left arch w.r.t the displacement, (d) mode weights variations of the right arch w.r.t the displacement, and (e) as-fabricated and deformed state of the arches at positions B, D, and G. In (c) and (d), the solid line corresponds to the loading path, and the dotted line represents the unloading path. In (e), the grey-dashed line shows the as fabricated shape, grey-solid line shows the deformed shape just before the position B, D, and G, and blue-solid line shows the deformed shape of the arches exactly at positions B, D, and G.

Conditions for switching. The switching point corresponds to the maximum force with respect to the displacement on the force-displacement curve, whereas the switchback point corresponds to the minimum force value. To get these switching points of the arch, we pose an optimization problem as follows.

$$\begin{aligned} &\underset{A_i s, B_i s}{\text{Maximize/Minimize}}: \quad F \\ &\text{subject to:} \\ &\qquad \frac{\partial\left(PE + \Lambda\Theta\right)}{\partial A_i} = 0 \\ &\qquad \frac{\partial\left(PE + \Lambda\Theta\right)}{\partial B_i} = 0 \\ &\qquad \Theta = 0 \end{aligned} \tag{14}$$

We numerically solve the preceding optimization problem to get the switching, switchback force, and their corresponding unknown mode weights, A_is and B_is so that they satisfy the equilibrium equations which are nothing but the KKT (Karush-Kuhn-Tucker) necessary conditions for the constrained optimization problem. The problem becomes easier when we consider only a few mode shapes to represent the shape of the arches. From our earlier studies [10], we found that the first three mode shapes are adequate to get accurate results. We call our semi-analytical modeling because we numerically solved the KKT conditions. In this short paper, details of the KKT conditions are not included due to paucity of space. We only present the results and their utility in ensuring flip-flopping of the arches.

When the load exceeds these limits, the load-bearing arch (say the left arch) switches to its inverted shape. However, the switching of the left arch does not guarantee the switching of the right arch. The switching of the right arch occurs when either the multiplier, Λ, exceeds the switching moment value of the right arch or the angular rotation of the left arch at $x = L$, $\left.\frac{dw_1}{dx}\right|_{x=L}$, crosses the critical angular rotation value of the right arch (see Fig. 6(b)). We get these critical switching moment and rotation value from the torque-rotation characteristics of the right arch alone when it is subjected to a concentrated moment at $x = 0$. For the particular arch considered here, the switching force and switchback force are 0.0315 N and 0.0075 N, respectively. We also found that the right arch switches to an inverted shape when the left arch switches, which is desired.

Conditions for bistability. The second stable state of the connected arch corresponds to a zero-force configuration other than the as-fabricated shape. Also, it represents a minimum on the strain energy landscape. To get the bistable configuration of the connected arches, we solve Eq. (11) to (13), by substituting $F = 0$. Once we get a solution, we check for the sufficiency condition to confirm the solution indeed has minimum energy. Therefore, we check the determinant of the principal minors of the bordered Hessian matrix, $\mathbf{H}_\mathbf{b}$, which is given by [12]

$$\mathbf{H}_\mathbf{b} = \begin{bmatrix} 0 & \nabla\Theta \\ \nabla\Theta^{\mathrm{T}} & \mathbf{H}\left(PE + \Lambda\Theta\right) \end{bmatrix} \tag{15}$$

where ∇ represents the gradient and $\mathbf{H}$ represents the Hessian of scalar functions. The value of the determinants of the principal minors become negative when the zero-force state corresponds to a stable configuration.

The nature of the connected arches depends on the as-fabricated shape of the individual arches. For certain values of mode weights, a_is and b_is, both the arches switch to their inverted shape when force and the multiplier exceed the threshold. But these arches may or may not be stable at their inverted shape. We can show from the determinant of the principal minors that it is necessary for the arches to be bistable individually to have an inverted second stable state when they are connected to each other. For the example we are considering, the arches are bistable individually, and they are bistable when they are connected. The studies on these connected arches are verified with the finite element simulation and presented in the next section.

3 Validation using finite element analysis

The force-displacement characteristics obtained from the analytical modeling shows good agreement (within 3% error at the switching and switch back point) with the results of finite element analysis (FEA). The comparison of these results for different as-fabricated connected arches are shown in Fig. 7. The solid curve represents the results obtained from the semi-analytical modeling considering five modes to approximate the deformed shape, and the dashed curve is obtained from FEA. The blue and the magenta curves represent the loading and unloading path, respectively. We have taken $h_{mid} = 10$ mm, $d = 1$mm, $b = 4$ mm, $L = 100$ mm, $E = 50$ MPa, and the poisson's ratio, $\nu = 0.35$ for all the examples. The FEA is performed in ABAQUS using continuum 2D quadrilateral elements, and the curve is obtained from the quasi-static dynamic-implicit analysis. Like the analytical modeling, FEA also shows different pathways for the loading and unloading cycle. Both the analyses show a kink at the switching and switchback point due to sudden asymmetric mode switching.

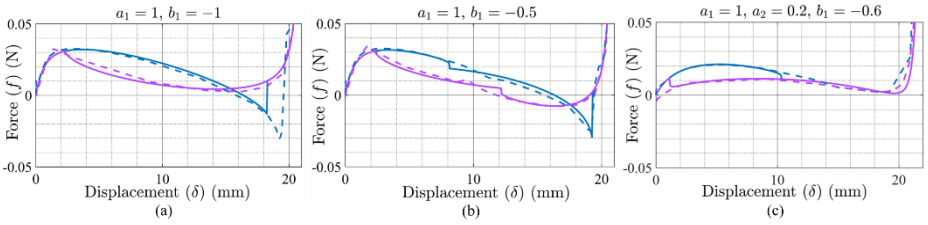

Fig. 7. Comparison of force-displacement characteristics with FEA for different as-fabricated shape, (a) configuration that does not switch to inverted shape and does not show bistability, (b) configuration that switches to inverted shape and shows bistability, and (c) configuration that switches to inverted shape but does not show bistability. The solid lines are the results from analytical modeling, and dashed lines are for FEA. The blue and magenta lines represent the loading path and unloading pathways, respectively.

For the example shown in Fig. 7a, when the mode weights are of equal magnitude in the as-fabricated shape, the right arch does not switch to its inverted shape and hence is not bistable. As we decrease the magnitude of the right arch, it switches and shows

bistability at the inverted shape, as shown in Fig. 7b. Both the analytical and FEA results show a sudden decrease in the slope when the left arch switch to its inverted shape. When we introduce asymmetric modes in the stress-free state, as in example Fig. 7c, the arches invert their shapes but return to their undeformed state as the load is removed, and hence are not bistable. The loss of stability occurs as the left arch does not have its force-free configuration other than the undeformed configuration. A similar analysis can be performed to get the equilibrium equations and stability conditions for the fixed-pinned arches, and the results can be compared with FEA in ABAQUS.

4 Closure

We presented a semi-analytical method to investigate the characteristics of connected arches. Using the equilibrium equations, we studied the characteristics of interconnected arches and observed different loading and unloading pathways for the connected arches. Based on the switching nature and stability conditions, we noticed three kinds of connected arches based on their as-fabricated shape: (i) When both the arches are identical and do not switch to their inverted shape, they are not bistable in the connected configuration; (ii) When we decrease the magnitude of first mode weight of the right arch to a certain limit, both the arches switch to their inverted shape, and the arrangement shows bistability; and (iii) The arch arrangement may flip but not be stable in their inverted configuration when any of the arches is not bistable individually. This analysis helps us in choosing the as-fabricated shapes of the connected arches for self-offloading footwear and other applications based on the corresponding design requirements.

Acknowledgment

The authors gratefully acknowledge the financial support from the Rajiv Gandhi University of Health Science (RGHUS), Karnataka, India. We also thank Jyoti S. Sonawane of Indian Institute of Science for proofreading the paper and giving valuable suggestions. Discussions with Dr. Pavan Belehalli of the Karnataka Institute for Endocrinology Research, Bengaluru, are also gratefully acknowledged in the clinical utility of the connected arches in novel footwear for diabetics.

References

1. Duckworth, T., Boulton, A. J., Betts, R. P., Franks, C. I., and Ward, J. D.: Plantar pressure measurements and the prevention of ulceration in the diabetic foot. J Bone Joint Surg Br, 67(1), 79–85 (1985).
2. Maharana, P., Sonawane, J., Belehalli, P., and Ananthasuresh, G. K.: Analysis of Planar Bistable and Snap-through Arches for Contact and Dynamic Loads. IFToMM WC 2019. Mechanisms and Machine Science, vol 73. Springer, (2019).
3. Maharana, P., Sonawane, J., Belehalli, P., and Ananthasuresh, G. K.: Self-offloading Diabetic Footwear Using Arrays of Snap-through Arches, Wearable Technologies, Cambridge Press (under review).
4. Palathingal, S., Ananthasuresh, G. K.: Analysis and design of fixed-fixed bistable arch-profile using a bilateral relationship. ASME Journal of Mechanism Robotics, Vol. 11, 031002-1. 1-18 (2019).

5. Palathingal, S., Ananthasuresh, G. K.: A bilateral relationship between stable profiles of pinned–pinned bistable shallow arches, International Journal of Solids and Structures, Vol. 143, 183-193, ISSN 0020-7683 (2018).
6. Vangbo, M.: An analytical analysis of a compressed bistable buckled beam, Sens. Actuators A 69 (3) 212–216 (1998).
7. Qiu, J., Lang, J. H., Slocum, A. H.: A curved-beam bistable mechanism, J. Microelectro-mech. Syst. 13 (2), 137–146 (2004).
8. Fung, Y. C., Kaplan, A.: Buckling of low arches or curved beams of small curvature, NACA, Washington, DC, United States, Technical Note 2840, 78 (1952).
9. Timoshenko, S. P., Gere, J. M.: Theory of Elastic Stability, 2nd edition. McGraw-Hill, New York (1988).
10. Palathingal, S., Ananthasuresh, G. K.: Design of bistable arches by determining critical points in the force-displacement characteristic. Journal of Mechanism and Machine Theory 117, 175-188 (2017).
11. Mead, D. J.: Free wave propagation in periodically supported infinite beams. Journal of Sound and Vibration, 11(2), 181-177 (1970).
12. Papalambros, P. Y., Wilde, D. J.: Principle of Optimal Design: Modeling and Computation, 2nd edition, Cambridge University Press (2000).